A computational study of structural and excitonic properties of chlorosomes

Li, X.

CHAPTER 1

A General Introduction

Photosynthesis begins with light-harvesting, where antenna complexes transform sunlight into electronic excitations that are subsequently delivered to reaction centers, where charge separation takes place and chemical energy is stored.[1,2] The efficiency with which these conversions are performed, and the amount of energy that is dissipated proceeding along the different steps in the conversion pathway, is of utmost significance for the functioning of photosynthetic organisms as a whole.[3,4] As a result, antenna complexes have developed in response to the environmental conditions that these photosynthetic organisms experience, which translates into specific features that ensure an optimal light-harvesting capability.[5,6] A very distinctive feature in the chlorosome structural antenna motifs is the amount of pigments that it contains, and their molecular and higher-order packings.[7,8] This unique type of antenna complexes has evolved at an early stage of evolution and allows photosynthetic green bacteria and some green filamentous anoxygenic phototrophs to survive under extreme low light-intensity conditions.[9,10] Chlorosomes are antenna assemblies containing hundreds of thousands bacteriochlorophyll (BChl) pigments and a small number of other light-active molecules. They are further distinctive with respect to other antennae in that they form their own responsive matrix without proteins.[11–16] This finding is intriguing and suggests that the efficiency of both the light-harvesting and exciton transport is *encoded* in the pigment assembly structure, in the absence of proteins. Elucidating the principles behind the efficient excitation energy transfer (EET) that takes place in chlorosomes will contribute to our understanding of photosynthesis[1,2,6,17–24] and may help to design artificial light-harvesting[25–28] or other optoelectronic

devices[29–32] with equivalent efficiency.

The lack of crystalline order in chlorosomes hampered detailed structure elucidation by standard x-ray diffraction techniques.[33] A challenge, particular to natural chlorosomes, is their heterogeneity in size, in overall shape, and in composition, which often strongly depends on the conditions in which they are grown.[15,34,35] To illustrate these challenges, I cite some comments taken from articles that represented the state-of-the-art at the start of my project in 2015: "the chlorosomes in green bacteria are the last class of light-harvesting complexes to be characterized structurally..."(2009, de Groot),[33] and "Since atomic details of chlorosomal antenna structures are not available (and probably never will)..."(2013, Linnanto and Korppi-Tommola).[36]

Structural information that did exist at the beginning of my project in 2015 was mainly a model for local pigment packing, the so-called *syn-anti* dimer packing model that will be discussed in more detail further on, that was first published in 2009 and derived from an analysis of solid-state nuclear magnetic resonance (NMR) spectroscopy data.[37] It provided a nice unit cell that could be employed for a helical tube model and structure prediction on a larger scale. The considered chlorosomes in this study were isolated from a mutant bacterium that contains significantly less heterogeneity in chemical composition and in overall structure. Additional information came from supramolecular structural level data from cryo-electron microscopy (cryo-EM) and their Fourier transformed counterparts, which provides the diffraction signal, for several types of chlorosomes of a rather homogeneous composition, either rich of BChl *c* or *d*.[15,37–39] In particular, the diffraction data provided the first clear evidence for the presence of tube chirality within the concentric tubular assemblies, in the form of a (weak) layer line[I], and estimates for the inter-tube stacking distances as well as the intra-tube spacing for different compositions.

This structural information, available at two levels of resolution, was then mapped onto a defect-free packing model for natural and mutant chlorosomes.[37] These resulting packing models are used as a basic assembly structure for many studies of chlorosomes.[35,40–46]

My overarching goal is to study how the coupling of atomistic and electronic

[I] The diffraction pattern of a helical structure is in the form of a series of layers of intensity, so-called layer lines.

degrees of freedom affects the transport efficiency of excitonic energy after sunlight is absorbed. Consequently, existing defect-free and static packing models were no longer sufficient, and we had to introduce irregularity and vibrational dynamics, or static and dynamic disorder, into a tubular molecular assembly that is preferably realistic. As apparent from the content of this thesis, we reached this goal by coupling all-atom molecular dynamics (MD) for the evolution of nuclear coordinates to a quantum mechanical (QM) description for the exciton diffusion. As a first step towards fully understanding functional mechanisms of chlorosomes, we studied the exciton dynamics in a quasi-closed system manner, see Chapter 4. As such, we have constituted an exotic hybrid QM/MM (quantum mechanics/molecular mechanics) approach that is quite general, and thus may find use also in other areas of research. The individual computational approaches are shortly discussed in section 1.3. Before reaching such a goal, we made substantial efforts to obtain realistic tube structures of chlorosomes. We bypassed the sampling limitations of MD for this system.[47] A reasonable **ansatz** we took is that chlorosomes in different species of bacteria may differ on a higher structural level, *i.e.* in terms of the fingerprint from cryo-EM diffraction and linear optical spectra, but share the same (*syn-anti*) packing unit. A pictorial summary of our strategies or an overview of the whole research content in this thesis is provided in Figure 1.1.

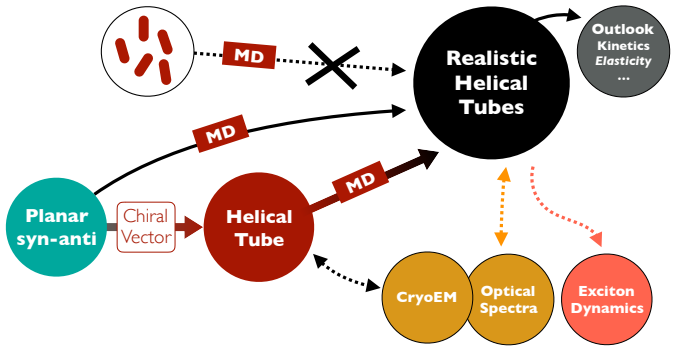

Figure 1.1: An schematic illustration of the strategies adopted in this thesis.

In Chapter 2, we report the results of MD simulations that identify key static and dynamic structural properties. To avoid kinetic trapping, which prevents the spontaneous formation of tube structures from disordered pigment molecules

at time scales that are accessible by all-atom MD simulation, we start from a planar assembly of (*syn-anti*) dimeric units *in vacuo*. We find that curvature spontaneously forms, showing that it is programmed into the local structure, and identify intrinsic dynamic structural heterogeneities involving molecular rotation and hydrogen bonding. In addition, we develop a theoretical analysis that allows us to identify chirality that matches the diffraction information obtained from cryo-EM, noting that this procedure does not provide unique chiral angles. To generate realistic full tubes with customized length, radius, and matching chiral angles, we developed a protocol, see Chapter 5, and an in-house code. This allowed us to verify that the molecular pigment motion that is observed in spontaneously formed curved sheets is the same as in a tube arrangement. In Chapter 3, we calculate linear optical spectra for realistic full tube structures for a direct comparison to experimental linear spectroscopy data, further narrowing down the set of chiral angles that were identified based on the layer line matching in Chapter 2. Our approach differs from a standard Frenkel Hamiltonian treatment in the sense that it includes actual disorder, taken from molecular conformations along the MD trajectory. Moreover, as opposed to the usual uncorrelated variation of the site energy, we incorporate these correlated variations into the electronic coupling between pigments. Although our treatment does not include dynamics on the quantum level, the results are shown to agree with several reported and proposed phenomena for chlorosomes, including exciton localization and level crossing. In particular, it provides the first molecular insight in the intricate mechanisms that underlie efficient energy transfer efficiency. In Chapter 4, we couple ground-state nuclear motion to exciton evolution, by considering a time-dependent Frenkel Hamiltonian, which follows the nuclear coordinates determined by MD, in the Schrödinger equation for exciton evolution. We find that disorder originating from thermal nuclear motions creates a fluctuating landscape for the localized exciton states and, as such, drives efficient transport of excitonic energy throughout the entire chlorosome. We note that our approach, as well as the insights it offers into the structural and excitonic properties of chlorosomes, can also be useful for other artificial tube assemblies.[48–50] It is recognized as a challenge to obtain realistic atomistic structures of full tubes formed by small organic molecules.[51] Such a difficulty hinders the understanding of such large tube molecular assemblies. For this reason, we shared our protocol for generating such realistic atomistic structures with highly customizable characteristics

in Chapter 5, and systematically analyze the relation between supramolecular chirality and optical response for chlorosome-like tubes. Such a detailed chirality-optical 'phase diagram' may be useful as a dictionary for optical spectroscopy characterization. Finally, in Chapter 6, we provide an extension of the current work towards mechanical properties and assembly kinetics in the form of an outlook, by reviewing unpublished results of significance. This may be useful for future research along the same directions.

1.1. Introduction to Chlorosomes

1.1.1. Photosynthesis

The significance of photosynthesis, and of photosynthetic research, for our daily life, in the form of the oxygen that we use, the vegetables we eat, our general well-being as well as the development of artificial devices for a more sustainable form of energy production, can not easily be overestimated.[17,52] Since my research has only focused on one aspect of photosynthesis, *i.e.* the chlorosome, I restrict myself to reviewing only the bare essentials. Photosynthesis, or more generally phototrophy, is the process in which (autotrophic) organisms convert radiant energy, and especially energy from light, into chemical energy stored in organic compounds.[52,53] The biological significance of photosynthesis is indisputable as it sustains the bottom of the food chain, and it dominates the global living atmosphere. These two aspects are vital for other (heterotrophic) organisms. Taking as an example plants, *i.e.* the most common photosynthetic organism seen in daily life, one may illustrate their importance by considering the following (from Hall and Coombs[54]): (i) "Each year plant photosynthesis fixes about 2×10^{11} tonnes of carbon with an energy content of 3×10^{21} J; this is about ten times the world's annual energy use and over two hundred times our food energy consumption", and (ii) "All the atmospheric CO_2 is cycled through plants every 300 years, all the O_2 every 2,000 years and all the H_2O every 2 million years.".

Item (ii) is also well demonstrated by considering a time trace of CO_2 concentration data.[I] As shown in Figure 1.2, this time trace shows an intriguing

[I] https://www.esrl.noaa.gov/gmd/ccgg/trends/global.html

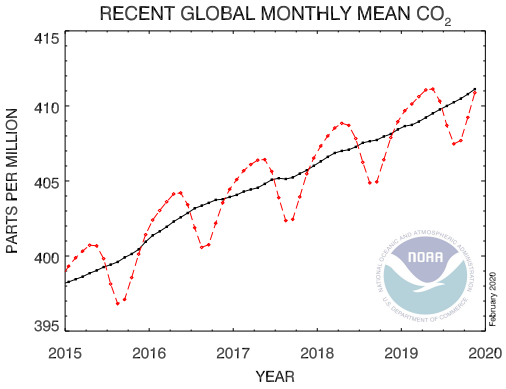

Figure 1.2: Monthly mean carbon dioxide globally averaged over marine surface sites presents seasonal oscillation. The dashed red line represents the monthly mean values. The black line represents the values after correction for the average seasonal cycle. Image provided by NOAA ESRL Global Monitoring Division, Boulder, Colorado, USA (http://esrl.noaa.gov/gmd/).

oscillatory behavior that matches the yearly seasonal cycle. It particularly illustrates the significance of natural photosynthesis for the composition of our atmosphere on a global scale.

1.1.2. Green Bacteria

Plants are the best-known photosynthetic organisms (autotrophs), but others exist, including certain types of algae and bacteria.[52] In particular, different types of organisms possess unique light-harvesting antenna to ensure survival and optimal energy harvesting efficiency in different inhabited environments.[6] Among these autotrophs, green bacteria, which include green sulfur bacteria *Chlorobi*, the phototrophic Acidobacteria "*Candidatus Chloracidobacterium*", and the filamentous anoxygenic phototrophs *Chloroflexi* (Figure 1.3),[16] are impressive for their survival ability in harsh environments, for instance in hot springs[55] and under low light conditions.[11,56,57] A special species of green sulfur bacteria even does not live off sunlight but from the infrared radiation from thermal vents nearly 2400 meters deep in the ocean.[12] The green sulfur

bacteria form the best-studied group, and especially *Chlorobaculum tepidum* (*C. tepidum*) has become as a model organism for the research of chlorosomes.[15] For this reason, we will also mostly concentrate on this particular group when referring the natural chlorosomes.

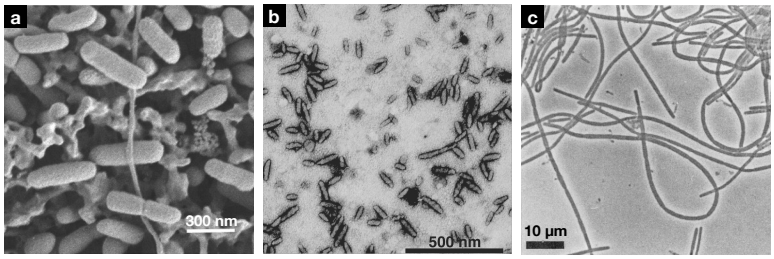

Figure 1.3: Images of different types of bacteria contain with chlorosomes.(a) TEM image of green sulfur bacteria. Figure reproduced with permission from ref [12]. Copyright 2005, National Academy of Sciences of the United States of America. (b) TEM image of *Candidatus Chloracidobacterium thermophilum*. Figure reproduced with permission from ref [58]. Copyright 2007, American Association for the Advancement of Science. (c) Photomicrograph of *Chloroflexus* aggregans. Figure reproduced with permission from ref [55]. Copyright 1995, International Union of Microbiological Societies.

1.1.3. General Information about Chlorosomes

An overall portrait of chlorosomes is given in Figure 1.4. In general, chlorosomes are located on the inside of the cellular membrane (as depicted in Figure 1.4a), and the term chlorosome refers to the organelle as a collection of tubes. Individual tubes are of an ellipsoidal shape, and display a considerable variation of shape and size, but on average they are 100–200 nm in length, and 40–60 nm in diameter.[15,16] Each chlorosome possesses a unique organization that is regulated by the conditions during formation, which is known to take place via a nucleation and growth mechanism.

An idea of the overall chlorosome shape can be obtained by transmission electron micrograph (TEM), see Figure 1.4a. Isolated tubes or molecular assemblies are composed of different types of molecules, with a total number in the order of 10^5, and as a whole wrapped by a lipid monolayer.[52,60] Molecular

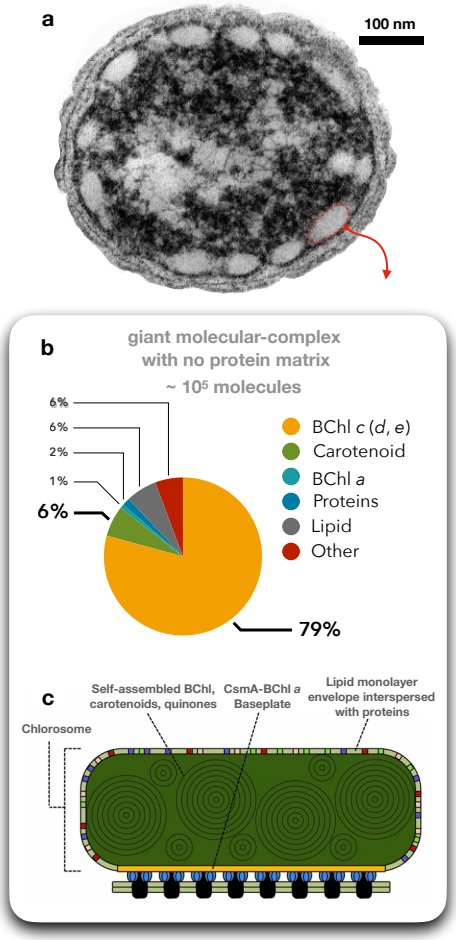

Figure 1.4: (a) TEM image of thin sections of the wild type *C. tepidum*. Figure reproduced with permission from ref [59]. Copyright 2002, American Society for Microbiology. (b) Illustration of typical chemical compositions of an ellipsoid chlorosome complex in green sulfur bacteria. (c) Schematic model of chlorosomes of green sulfur bacteria. Figure reproduced with permission from ref [16]. Copyright 2013, Springer Nature.

ratios in the composition vary with species and growth conditions. The main body, which we refer to as the chlorosome here and further on, is mainly composed of BChl *c/d/e* pigments and contains a small amount of carotenoid molecules, but no proteins, which are only present in the lipid monolayer, see Figure 1.4b. An assembly containing BChl *a* and proteins forms the two-dimensional baseplate that connects the chlorosomes to the next components in the energy transport chain: the Fennna-Matthews-Olson (FMO) complex and the reaction center. Figure 1.4c shows a schematic representation of the chlorosome of green sulfur bacteria. The energy levels for different light-harvesting components in green sulfur bacteria are in a decreasing order, introducing a driving force for energy transfer from chlorosomes to reaction centers.[61,62]

1.2. The Dawn of Atomistic Tube Structure of Chlorosomes

The *syn-anti* Packing Tube Model. The local structure of the chlorosome, the so-called *syn-anti* model mentioned before, was first determined by matching NMR chemical shifts, which give rise to distance constraints to the molecular structure of a molecule with two neighbors from the stack, and further validation by density functional theory (DFT) calculations.[37] A dimeric unit cell was found composed of one molecule in the *syn* and the other in the *anti* conformation, with the electronic dipoles in a staggered parallel orientation, see Figure 1.5. The necessary ingredient for this investigation was the availability of chlorosomes of a reduced structural heterogeneity due to a significantly homogeneous chemical composition, a condition that was satisfied by chlorosomes isolated from *bchQRU* mutant of *C. tepidum*, which are composed of >95% BChl *d* pigments. Next, cryo-EM images taken from this chlorosome first confirmed a concentric tube morphology and allowed for a determination of a 2.1-nm layer spacing between BChl layers. Additionally, the diffraction signal, obtained by Fourier transformation of the cryo-EM images, identified a relevant 0.85 or 1.21 nm periodicity for the mutant type or wild type chlorosome tube structure for a single but weak layer line, confirming that the molecular packing is more irregular or non-crystal-like on a larger scale (Figure 1.5b).

Based on this information, regular tube models that satisfy these two structural constraints were proposed (Figure 1.5c). In the more general framework, these tubes can be obtained by rolling a planar lattice of *syn-anti* unit cells along a rolling vector into a curved lattice on a tube. For more detail on this general procedure and on the correspondence of the resulting helical families and the scattering pattern, we refer to the literature [63]. Consequently, this rolling or chiral vector uniquely defines the resulting tube structure. For instance, the proposed tube model for the mutant type[37] means that it is rolled along the *syn-anti* stacks. In this thesis, we develop an approach for more generally relating scattering signals to the direction of rolling, assuming that the chlorosomes from different bacteria species share the same *syn-anti* packing unit. It agrees with the tube models that existed before the project in the sense that we also assume that chlorosomes only differ in their particular chiral vector that sets the chirality of the tube.[37]

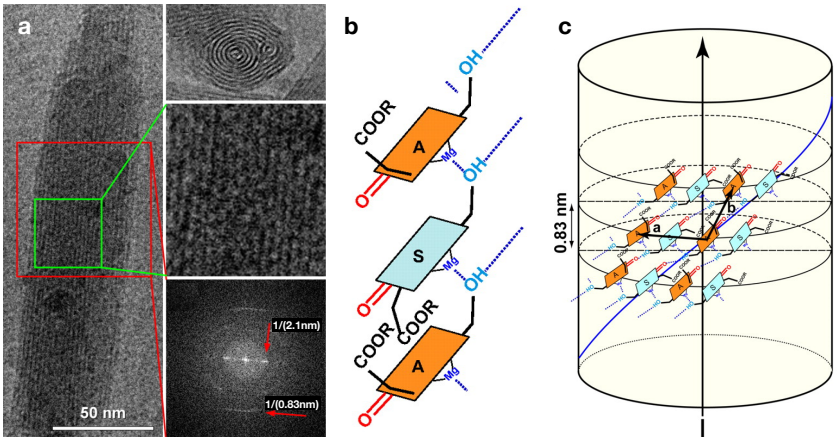

Figure 1.5: The *syn-anti* packing model.[37] (a) Cryo-EM images. (b) The *syn-anti* stack structure. (c) A tube model for *bchQRU* mutant *C. tepidum* chlorosomes. Figures reproduced with permission from ref [37]. Copyright 2009, National Academy of Sciences of the United States of America.

The *syn-anti* packing model is visually summarized in Figure 1.6. To better understand the process of building a structure from the *syn-anti* unit cell, I encourage the reader to check the movie showing how to duplicate these

packing units, see the supporting information.[I] Concentrating on an even smaller unit, *i.e.* the molecular building blocks themselves, we note that the BChl *c/d/e* molecules only differ in some side groups, and that we may envision such a molecule composed of a rather rigid head and a flexible farnesyl tail. In the movie, we have represented each molecular head part in a simplified or minimal form as a disc. Similarly, the hydroxyl side group, which determines the molecule's internal chirality (*syn* or *anti*), can be represented as a red sphere, see Figure 1.6, while the red triangle denotes a carbonyl group that can form a hydrogen bond with this hydroxyl group. The *syn-anti* dimeric structure is defined as follows: when the hydroxyl group is at the same side as the wedge bond (green in Figure 1.6), the configuration is denoted as *syn*, while it is denoted as *anti* when they are in the opposite directions. On a larger scale, BChl stacks are stabilized by a network of local interactions: the coordination interaction between Mg and O atoms, hydrogen bonding interactions, and π-π stacking of head parts, see also Figure 1.6. The flexible tails of each molecule cover both sides of the stacks and fill the interstitial space between different layers in the concentric tube topology, as further discussed in Chapter 2. We note that BChl *a* and *f*, which are no natural components of chlorosomes, lack the hydrogen bonding interactions. We also note that the parameters (a, b, γ) corresponding to the underlying (loose) 2D unit cell lattice are not experimentally available and will be estimated from MD simulations.

1.3. Computational Preliminaries

1.3.1. MD Simulation and Its Proper Usage

In classical atomistic simulation by MD, many-body interactions in a system composed of electrons and nuclei are mapped onto effective potentials for a system composed of only nuclei. In such a representation, electrons are assigned as an additional property — charge parameters — to each nucleus. Atomic masses and the atomistic forces that are derived from these effective potentials are then used to evolve the nuclear positions in time, a process that is governed by Newtons classical laws of motion. A typical analytical

[I] File syn-anti-model.mp4 in chapter_1 folder at https://github.com/xinmeng2015/chlorosome_phd_thesis or https://doi.org/10.5281/zenodo.3674742

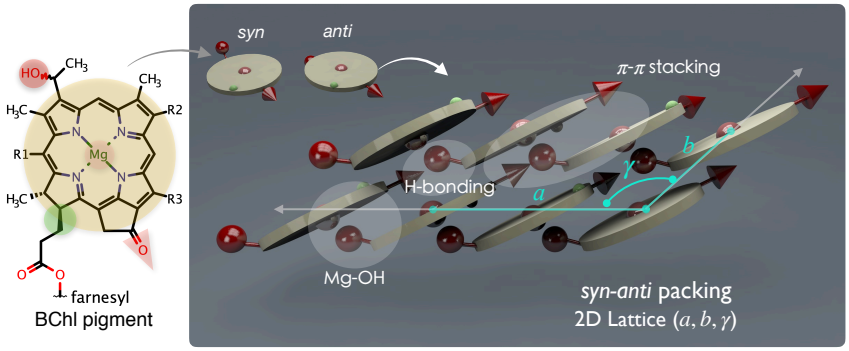

Figure 1.6: A simplified disc model of the *syn-anti* packing model. The macrocycle ring of a BChl is referred to as the head, which is visualized as a disk. The farnesyl chain of a BChl is referred to as the tail, which is omitted in the packing model.

form of the force field is composed of bonded terms, representing chemical bonds, angles and dihedrals, and non-bonded terms, representing van der Waals and electrostatic interactions. There are several popular force fields for organic/biological molecules,[64,65] *e.g.* AMBER, OPLS and GROMOS. For further technical details of MD simulations, I refer to a nice book, *The art of molecular dynamics simulation*.[66]

Owing to the optimized and readily available MD simulation packages like GROMACS, NAMD and LAMMPS, and supported by the accessibility of large parallel supercomputers at central high-performance Computing Centers, performing large-scale MD simulations is nowadays relatively straightforward. However, one should not take for granted that simple "brute force" simulations will solve all your molecular puzzles. In particular, one will often experience that, starting from an arbitrary disordered state, the ability of MD to sample all relevant parts of the phase-space is largely insufficient to identify structures or phenomena that can be matched to experimental observations. Especially for large biological or bio-inspired supramolecular systems, simple "brute force" simulation may, and often will fail, as reviewed by the Marrink's group.[51] There are various reasons for this failing, an important one being that the van der Waals interactions contain an attractive well, which generates numerous local minima that will always hinder the sampling. In particular, when aggregates grow from nucleation, positional adjustment within the aggregates becomes

increasingly difficult and the process of equilibration experiences a critically slowing down phenomenon, with characteristic time scales that become very large. Therefore, computational research of chlorosomes, or similar aggregates with unique mesoscopic/macroscopic order, requires careful consideration of the starting structure, preferably incorporating experimental information. We do not suggest to run MD simulations from totally disordered structures, see the disorganized aggregates we obtained in Figure 1.7. Instead, it is recommended to start from a structure making use of known constraints. For instance, in Chapter 2, we started from a pre-packed planar structure in vacuum. The MD simulation induces spontaneous curvature, a phenomenon that can not be observed by energy minimization methods.[67] Besides, in Chapter 3, starting from pre-packed full tube structures, the MD simulation will equilibrate the structure and introduce intrinsic structure disorder, and thus generate useful ground-state nuclear motions.

To address the kinetics of chlorosome formation, the system should be simulated on a much longer time scale, possibly even on a macroscopic time scale of minutes and hours. Unique coarse-grained models can be tested to see if this is an option, see a brief discussion in Chapter 6.

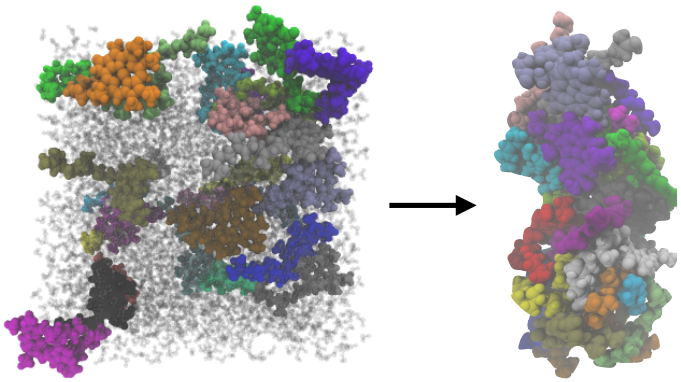

Figure 1.7: Unstructured aggregate of BChl *d* molecules obtained by a 15-ns MD simulation. Initially, the pigments (identified by different colors) are mixed randomly with water molecules (gray). The assembly structure remains stable with elongated simulation time.

1.3.2. Frenkel Exciton and Linear Optical Spectra

Pigments are chemical compounds that can absorb light of an appropriate wavelength. Popular types of pigments found in natural light-harvesting complexes include chlorophylls(Chl), BChl, and carotenoids.[26] When a single pigment absorbs light, it goes from a ground state to an excited state. Although such a monomeric case can in principle be described by time-dependent density functional theory (TDDFT), the situation changes when pigments are coupled together by being closely packed into a solid aggregate. In such a situation, they get excited collectively, see Figure 1.8, and the exciton thus becomes delocalized.[68] The number of pigments, and thus of nuclei and electrons, involved in such a delocalization strongly prohibits the application of "brute force" quantum methods for electronic structure calculation. Instead, the problem can be reformulated in terms of an effective Frenkel exciton Hamiltonian for exciton energy transfer in molecular aggregates, which separates aggregates into Coulomb-coupled monomers, and represents a convenient framework for simulating large-scale electronic excitations.[69,70] The Frenkel exciton Hamiltonian is widely used to study excitations and exciton evolution in molecular crystals, conjugated polymers, organic photovoltaics, photosensitizers, and light-harvesting complexes in photosynthesis.[71]

In a Frenkel exciton treatment, each molecule is represented as a single site, and the interplay/coupling between different molecules is described by a single parameter, the coupling strength. In general, a Frenkel exciton Hamiltonian $\hat{H}$ for a system composed of N molecules is an N by N matrix:

$$\hat{H} = \sum_i \nu_i \, |i\rangle\langle i| + \sum_{i \neq j} J_{ij} \, |j\rangle\langle i| \qquad i, j \in [1, N]. \tag{1.1}$$

The expression of $\hat{H}$ is adapted slightly in Chapters 3 and 4 where the dependence of the $\hat{H}$ on the nuclear positions or the positions of transition dipoles is emphasized. The diagonal term ν_i represents the monomer excitation energy of the i-th molecule. Off-diagonal terms J_{ij} represent the coupling between excited states of the i-th and j-th molecules, which is also referred to as the electronic (or excitonic) coupling between the i-th and j-th molecules. For a given molecular system of restricted size, *e.g.* for the FMO complex, the site energy ν_i and the coupling strength J_{ij} for each molecule/site can be deter-

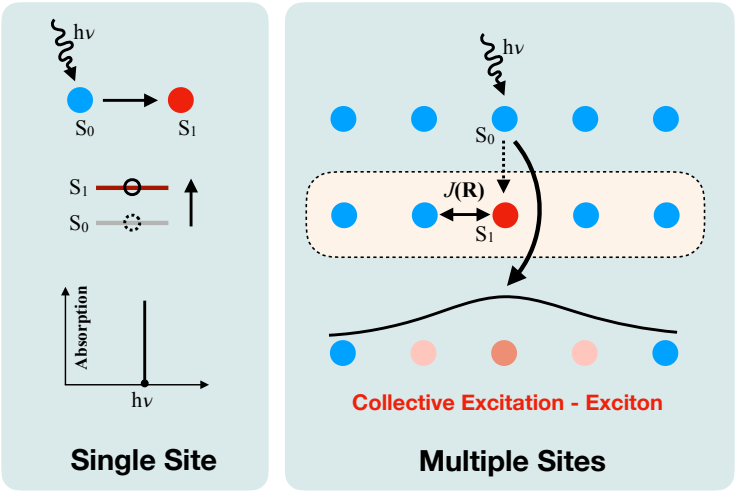

Figure 1.8: From monomeric excitation to collective excitation. The coupling strength $J(\mathbf{R})$ determines whether the excitation energy is blue (or red) shifted compared to the monomeric excitation, which defines the aggregate as an H (or J) type.

mined with good precision using quantum chemical calculations,[72–77] and used to study the exciton evolution on longer length scales, which is discussed in detail in Chapter 3. Chlorosome-like assemblies of a realistic size, however, are composed of closely packed pigments, meaning that the system size that has to be considered for obtaining reliable parameter values rules out full QM approaches. In consistency with previous chlorosome studies, we therefore consider the experimentally measured site energy and calculate the coupling strength from the standard point-dipole approximation (PDA):

$$J_{ij} = \frac{\boldsymbol{\mu}_i \cdot \boldsymbol{\mu}_j}{\left|\mathbf{R}_{ij}\right|^3} - 3\frac{(\boldsymbol{\mu}_i \cdot \mathbf{R}_{ij})(\boldsymbol{\mu}_j \cdot \mathbf{R}_{ij})}{\left|\mathbf{R}_{ij}\right|^5}\,, \tag{1.2}$$

with $\boldsymbol{\mu}_i$ the effective transition dipole moment vector for the i-th molecule and $\mathbf{R}_{ij}$ the distance vector between the two transition dipoles labeled by i and j. The expression of J is adapted slightly in Chapters 3 and 4 where the dependence of the J on the nuclear positions or the positions of transition dipoles is emphasized.

Diagonalization of the Hamiltonian matrix (1.1) provides N eigenvectors $|\psi_m\rangle$ and eigenvalues ε_m that correspond to stationary exciton states and excitonic transition energies,[I] *i.e.* $\hat{H}\,|\psi_m\rangle = \varepsilon_m\,|\psi_m\rangle$. For a system described by a static $\hat{H}$, the wave functions $|\psi_m\rangle$ are the instantaneously allowed "exciton orbitals" that accommodate the energy of the absorbed photons.

Spectra Calculation. Optical spectra for chlorosomes have been measured experimentally. These spectra, although even not always matching for similar chlorosomes, share several properties: a large red-shift in the absorption (OD) spectra, a dominant positive peak in linear dichroism (LD) spectra and a psi-type shape in circular dichroism (CD) spectra, see Chapter 3. To further narrow down the set of matching chiral angles for chlorosomes, and to understand this experimental variability, we calculated linear spectra for the whole set of candidate chiral angles that were obtained after matching the layer line position. We follow the Frenkel exciton Hamiltonian treatment, and note that each exciton state $|\psi_m\rangle$ corresponds to a (stick) signal amplitude, *i.e.* d_m for absorption, LD_m for LD and $\mathcal{R}_m$ for CD, computed using Eq. 1.3, for the eigenvalue or energy ε_m on the horizontal axis, with[36,78–80]

$$\begin{aligned} d_m &= \sum_{i,j=1}^{N} (\boldsymbol{\mu}_i \cdot \boldsymbol{\mu}_j) c_{mi} c_{mj} \\ LD_m &= d_m^{\parallel} - d_m^{\perp} = \frac{1}{2} \sum_{i,j=1}^{N} [3(\boldsymbol{\mu}_i \cdot \mathbf{e})(\boldsymbol{\mu}_j \cdot \mathbf{e}) - \boldsymbol{\mu}_i \cdot \boldsymbol{\mu}_j] c_{mi} c_{mj} \\ \mathcal{R}_m &= 1.7 \cdot 10^{-5} \sum_{i,j=1}^{N} \varepsilon_m [\mathbf{R}_{ij} \cdot (\boldsymbol{\mu}_j \times \boldsymbol{\mu}_i)] c_{mi} c_{mj} \end{aligned} \tag{1.3}$$

Here, c_{mi} represents i-th element of $|\psi_m\rangle$ with $c_{mi} = \langle i|\psi_m\rangle$, and $\mathbf{e}$ is a unit vector along the long axis of the tube.

[I] One should be careful about how the multidimensional array data are stored. For instance, in the diagonalization function I used, scipy.linalg.eigh, the output eigenvectors are stored as column vectors, following the column-major order format in Fortran language.

1.3.3. Quantum Dynamic Simulation of Exciton Evolution

Compared to classical mechanics, where particles move according to Newton's laws of motion, in quantum mechanics, wave functions propagate according to the time-dependent time-dependent Schrödinger equation[81]

$$i\hbar\frac{\partial}{\partial t}|\psi(t)\rangle = \hat{H}|\psi(t)\rangle\,. \tag{1.4}$$

Just as mass is an essential property of particles in the classical domain, energy is a crucial property for wave functions. We only consider closed quantum systems, meaning that the total energy is conserved due to the absence of any form of dissipation. Non-stationary evolution takes place when $|\psi\rangle$ is a mixture of different stationary states $|\phi_i\rangle$ of the Hamiltonian $\hat{H}$, for instance, $|\psi\rangle = c_1\,|\phi_1\rangle + c_2\,|\phi_2\rangle$. In such a case, the unitary evolution of $|\psi(t)\rangle$ governed by Eq. 1.4 gives rise to a time-dependent density matrix $\rho(t)$

$$\begin{aligned}\rho(t) = |\psi(t)\rangle\langle\psi(t)| = |c_1|^2\,|\phi_1\rangle\langle\phi_1| + |c_2|^2\,|\phi_2\rangle\langle\phi_2| \\ + c_1c_2^*e^{-i(E_1-E_2)t/\hbar}\,|\phi_1\rangle\langle\phi_2| \\ + c_1^*c_2e^{-i(E_1-E_2)t/\hbar}\,|\phi_2\rangle\langle\phi_1|\,.\end{aligned} \tag{1.5}$$

The first two (diagonal) terms represent populations in the exciton state basis, and the latter two (off-diagonal) terms describe coherences.[23] The phase factors in the coherence terms determine the population variation in the site basis, and give rise to an oscillating exciton evolution in real space. In particular, the frequency of this oscillation depends on the energy difference $\Delta E = E_1 - E_2$ and increases when ΔE increases. If we additionally would concentrate on interactions with the environment, *i.e.* an open quantum system, energy dissipation, and loss of coherence due to decoherence effects will modulate the density matrix $\rho(t)$ in Eq. 1.5. In this thesis, however, such non-stationary effects are not considered. Instead, we study the role of ground-state nuclear motion by using a time-dependent Hamiltonian $\hat{H}(t)$ and solve $i\hbar\frac{\partial}{\partial t}|\psi(t)\rangle = \hat{H}(t)|\psi(t)\rangle$. This Hamiltonian $\hat{H}(t)$ is constructed from a fully in parallel propagating classical molecular description of the same system on which the quantum evolution is considered, which is coupled by exchanging the nuclear information that is required for computing the $J(t)$ contribution to $\hat{H}(t)$ at discrete Δt, *e.g.* 20 fs, intervals. We note that, although $\hat{H}(t)$ has now indeed become time-dependent,

this dependence is in practice rather weak on a short time interval of 20 fs between consecutive updates, owing to the minute variations in intermolecular distances and induced dipole moments that take place on such a time scale. For this reason, we have considered a constant $\hat{H}(t)$ between updates, see also ref [82, 83] and details in Chapter 4, which simplifies the calculation of the wave function evolution by time integration of $i\hbar\frac{\partial}{\partial t}|\psi(t)\rangle = \hat{H}(t)|\psi(t)\rangle$. We note that reverse coupling, *i.e.* including the effect of excitation on the nuclear motion, is lacking. This is in line with the usual assumption that molecular reorganizations due to excitation, as signaled by the Stokes shift, are minor and can be neglected, which is particularly the case in the context of our effective Frenkel description.